Modelling and Comparing Converter Architectures and Energy Harvesting ICs for Battery-Free Systems

Hannah Brunner, Sebastian Scholl, Carlo Alberto Boano, and Kay Römer
Institute of Technical Informatics, Graz University of Technology, Austria
Email: hannah.brunner@tugraz.at, s.scholl@student.tugraz.at, cboano@tugraz.at, roemer@tugraz.at

***Abstract*—Battery-free energy-harvesting devices are a new class of embedded systems that operate from ambient energy stored in environmentally-friendly capacitors and promise long-lasting, maintenance-free operation. Due to tight energy constraints, these devices often employ voltage converters and dedicated integrated circuits (ICs) to maximize the power transfer between energy harvester, storage capacitor, and load. As we show in this paper, the selection and configuration of such converter circuits are important, but non-trivial, as their performance is highly dependent on the energy harvesting conditions. We thus provide models of five off-the-shelf energy harvesting ICs and integrate them into an open-source simulator for battery-free systems: this allows practitioners and researchers to conveniently explore the design trade-offs and anticipate the achievable performance. Furthermore, we use these models to perform a systematic comparison of different converter architectures and derive concrete recommendations.**

I. Introduction

The Internet of Things (IoT) connects a great number of devices monitoring the environment in an unprecedented way. A large portion of these devices is battery-powered and thus has inevitable drawbacks such as high maintenance costs and environmental impact. To overcome these disadvantages, *battery-free devices* powered by ambient energy (e.g., solar, thermal) have emerged as a viable alternative and promise long-lasting, maintenance-free operation [1], [2].

Battery-free devices use energy harvesters to extract energy from the environment and store it in small capacitors that power an IoT node. The design of such devices is difficult, as the small amount of available ambient energy together with the limited storage capacity require the devices to be as energy-efficient as possible. This is particularly challenging considering that each device component might exhibit different optimal operating points. For example, energy harvesters can extract the maximum amount of energy only at a certain operating voltage (i.e., the so-called maximum power point (MPP) [3]), while loads typically have to operate within given voltage limits. If the harvester, load, and capacitor are directly connected, they all share the same operating point and might run outside of their ideal conditions, which reduces the overall performance or, in the worst case, renders the system unusable.

DC/DC converters to maximize efficiency. To overcome this problem, one or more DC/DC converters can be employed and allow each component to run at a different voltage level [4]. The latter is especially beneficial for common energy harvesters (e.g., solar panels), as their MPP depends on environmental conditions (e.g., temperature and irradiance) and changes over time. There exist techniques that periodically determine the MPP and control an (adaptive) DC/DC converter accordingly, thus increasing the energy harvesting efficiency substantially [5]. Several manufacturers have integrated such approaches into dedicated low-power energy-harvesting integrated circuits (EH-ICs) [6]–[9] that allow charging the capacitor even from extremely small input power (i.e., tens of μW) while providing a constant output voltage to the load.

Selection of energy harvesting ICs is non-trivial. Despite the advantages gained in energy harvesting performance, these ICs introduce several drawbacks such as increased complexity, size, and costs, as well as non-neglectable start-up times [10]. Additionally, as the MPP tracking mechanism and voltage conversion themselves consume a small amount of energy, it is not necessarily the case that the IC's benefits outweigh the additional losses. While in scenarios with little available ambient energy a harvesting IC might be indispensable to allow the device to operate at all, its losses can have a negative impact on the system's performance in favorable energy environments. More specifically, as we show in this paper, directly coupled systems (i.e., without any DC/DC converter) can be more efficient in certain configurations. Using the same harvesting input, a converter-less system features up to 40% lower charging times and 94% faster start-up times (i.e., charging times from a cold start). Furthermore, there exist large differences across the different types of energy-harvesting ICs: at the same energy harvesting conditions, ICs might exhibit start-up times that differ by a factor of up to 15.

These circumstances make the decision *whether* to use energy harvesting ICs or DC/DC converters and in *which* exact configuration an important but non-trivial task.

Simulation to facilitate design decisions. To accelerate and simplify such design decisions, developers often resort to simulation, which enables fast design space exploration without access to real hardware [11]–[13]. Although several simulators targeting battery-free devices are available [11], [13], [14], they are commonly designed for converter-less systems and thus cannot support the simulation of different converter architectures. Furthermore, there are hardly any models of off-the-shelf energy harvesting ICs available that can be integrated with such simulators, as the creation of converter models typically involves time-consuming and measurement-heavy data collection. Consequently, there are so far only models of a single converter-family (i.e., TI BQ255xx) available [15], and these include only limited operating modes.

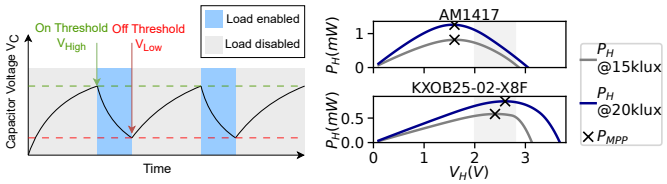

(a) Intermittent operation of a battery-free device

(b) P-V characteristics of two solar panels

Fig. 1. Typical operation of a battery-free IoT node (a) and examples of P-V curves of two different solar panels (b).

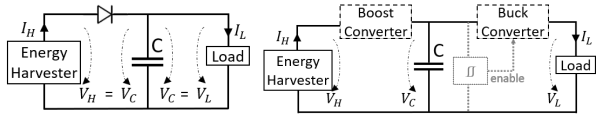

(a) Converter-less architecture

(b) Converter-based architecture(s)

Fig. 2. Typical architectures of battery-free IoT nodes. In a converter-less architecture, the harvester, capacitor, and load are directly coupled and share the same voltage. In converter-based architectures, one or more voltage converter(s) decouple the capacitor from the harvester and/or the load.

Given the difficult evaluation process of battery-free systems and the lack of converter models, there exists yet no study that explicitly *compares converter architectures and different energy harvesting ICs* for battery-free IoT nodes.

Our contributions. In this work, we fill this gap and provide a comparison of converter architectures and several energy-harvesting ICs for battery-free IoT nodes. To this end, we model three different off-the-shelf energy harvesting chips and two DC/DC converters based on a measurement campaign using real hardware. We integrate these models into the Simba simulator, make them available in Simba's open-source repository [16], and verify their accuracy experimentally.

Furthermore, we use the models to perform a quantitative comparison of the different architectures and energy-harvesting ICs in simulation. Based on the simulation results, we discuss the advantages and shortcomings of the different solutions, ultimately deriving concrete recommendations.

II. Battery-Free IoT Nodes and their Different Converter Architectures

Battery-free devices are commonly composed of a small energy harvester, a storage capacitor, a load (i.e., the IoT node itself), as well as optional voltage converter and monitoring circuits. Although ambient energy is in principle unlimited, its temporal availability and power density are often low, which forces battery-free devices to operate *energy-driven* [17], i.e., on a tiny energy budget or even *intermittently* [1] through frequent power failures, as depicted in Fig. 1a.

A. Architectures

Battery-free IoT nodes employ different architectures, depending on the presence of DC/DC converters within the system. Each architecture features distinct (dis)advantages and should be chosen according to the application requirements.

Converter-less architecture. In its simplest form, a battery-free device uses a converter-less architecture, where the energy harvester, the capacitor, and the load are directly connected, as shown in Fig. 2a. While this architecture minimizes size, costs, and converter losses, it is rather inflexible and can introduce inefficiencies due to the shared operating point of the components (i.e., $V_H{=}V_C{=}V_L$). Consequently, as the IoT node's load can only operate within a certain voltage range (typically 1.8-3.6V), the harvester's output voltage must exactly match these requirements to enable the load's operation and to protect it from overvoltage. Furthermore, many harvesters exhibit non-linear I-V characteristics, which means that the harvesting current I_H (and hence the power P_H) depend on the applied voltage [3], as shown in Fig. 1b. Given that the harvester's operating point is directly affected by the state of charge of the capacitor, the harvester might operate outside of its optimal conditions and thus deliver poor harvesting efficiency.

Converter-based architectures. To relax these dependencies, different converter-based architectures can be applied, where one or more DC/DC converter(s) are used to decouple the components' operating voltages (see Fig. 2b). In general, converter-based systems increase efficiency and design flexibility, as the harvester must not match the load's voltage specification. However, DC/DC converters also introduce drawbacks such as increased costs, complexity, as well as converter losses, and the so-called cold-start problem, as explained next.

Boost-only architecture. In a boost-only architecture, a single DC/DC converter is placed between the harvester and capacitor to control the harvester's voltage independently of the capacitor's state of charge. This way, the harvester can operate at its MPP to maximize the harvested power (see Fig. 1b), while still charging the capacitor to higher voltages. As the harvester's I-V characteristics change depending on environmental conditions and temperature, the DC/DC converter is commonly controlled by an accompanying MPP tracking (MPPT) logic, which adapts the harvester voltage accordingly.

Although energy harvesting ICs embedding MPPT can improve the harvesting efficiency significantly, they require a minimum voltage to operate properly and thus suffer from the *cold-start problem* [18]. At cold start, i.e., if the capacitor is empty, the ICs can only extract energy if a certain minimum harvesting voltage $V_{CS,min}$ is applied. Furthermore, in cold-start mode (i.e., as long as the capacitor voltage remains below the IC's operating voltage), the harvesting efficiency is commonly very low and thus the overall system experiences non-neglectable start-up times that affect device availability.

Buck-only architecture. In a buck-only architecture, a buck converter regulates the capacitor voltage down to a constant output voltage that drives the load. This means that the capacitor can be charged to voltages exceeding the load's specification, which increases the capacitor's storage capacity. Furthermore, operating the load at a fixed, low voltage level can improve device efficiency and facilitate system modelling.

Buck-boost architecture. Finally, several existing energy harvesting ICs [6], [7], [9] employ a buck-boost architecture, where both DC/DC converters are employed, combining the (dis)advantages of each architecture.

TABLE I
USED ENERGY HARVESTING ICS (EH-IC) AND DC/DC CONVERTERS

Name	Type	Architecture	MPPT	Load switch	Voltage monit.
MAX20361	EH-IC	Boost-buck	✓	✗	✗
BQ25570	EH-IC	Boost-buck	✓	✓	✓
AEM10941	EH-IC	Boost-only	✓	✗	✓
TPS7A02	LDO	Buck-only	✗	✗	✗
XC9265	Step-down	Buck-only	✗	✗	✗

B. Voltage monitoring and load switch

Apart from DC/DC converters, battery-free IoT nodes may also employ voltage monitoring circuits (e.g., to inform the load about expected power failures) and comparator-driven load switches (as depicted in grey in Fig. 2b). Load switches are popular in intermittent systems [4], [19], [20] to enable and disable the load at certain capacitor voltage thresholds.

III. MODELLING ENERGY HARVESTING CHIPS

In order to explore the performance of converter architectures and energy-harvesting ICs on the overall system performance of a battery-free device, we extend the Simba simulation framework [13] with models of several off-the-shelf ICs. Simba is an open-source framework for battery-free devices that allows an investigation of the complex interplay between device components using discrete-time simulation, not yet offering support for different real-world converter ICs.

Selected components. In this study, we create Simba-compatible models for three different popular energy-harvesting ICs, namely the Texas Instruments BQ25570 [6], ePeas AEM10941 [7], and Analog Devices MAX20361 [8], as well as two types of low-power DC/DC (buck) converters, i.e., the TI TPS7A02 low-dropout regulator (LDO) [21] and the Torex XC9265 step-down converter [22]. As summarized in Tab. I, the selected ICs offer different feature sets and cover – together with Simba's built-in support for converter-less systems – all common architectures described in Sec. II-A.

A. Modelling energy harvesting ICs

A typical EH-IC embeds DC/DC converters that exhibit different input/output voltages (V_H, V_L) as well as voltage conversion efficiencies (η_H, η_L) depending on their operating conditions and operation mode (m). In battery-free devices, as sketched in Fig. 2, these conditions depend on the harvester's input current and open-circuit voltage (I_H, V_{OC}), the capacitor's state-of-charge ($\propto V_C$), and the load's current consumption (I_L) [13], [15]. The IC can thus be modelled using

$$V_H = f_{H,IC}(V_C, V_{OC}, m),\ \eta_H = f_{H,IC}(V_C, V_H, I_H, m) \quad (1)$$

for the boost-conversion (i.e., on the harvester side) and

$$V_L = f_{L,IC}(V_C, m), \eta_L = f_{L,IC}(V_C, V_L, I_L, m) \quad (2)$$

for the buck-conversion (i.e., to the load), respectively.

Modes of operation. The core functionality of common energy harvesting ICs can be modelled using four different modes of operation, as depicted in Fig. 3.

Cold-start mode. In cold-start mode, the capacitor voltage V_C is smaller than the IC's minimal operating voltage $V_{IC,min}$ and thus too small to power the IC for normal operation. As a result, the buck converter is disabled (i.e., $V_L = \eta_L = 0$) and the boost converter operates with low efficiency in a chip-specific cold-start mode.

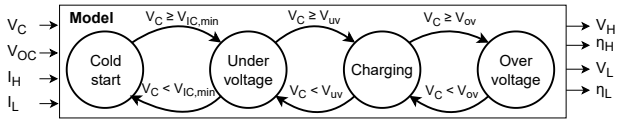

Fig. 3. State machine of the energy harvesting ICs' modes of operation.

Under-voltage mode. Once the IC leaves cold-start mode ($V_C > V_{IC,min}$), the boost converter can operate normally and sets the input voltage according to the MPPT functionality. More specifically, the IC periodically measures the harvester's open circuit voltage V_{OC} and regulates the converter's voltage to $V_{MPP} = kV_{OC}$, where k is a harvester-specific constant that is configurable. The buck converter remains disabled until the under-voltage threshold V_{UV} is reached to prevent the IC from falling back into cold-start mode.

Charging mode. In charging mode, both the boost and buck converter are enabled simultaneously and operate normally. The buck converter's output voltage V_{OUT} is typically a fixed value that is configurable using resistor networks and can be set according to the load's voltage specification (see Eq. (3)).

Over-voltage mode. To prevent the capacitor from over-charging, energy harvesting ICs enter over-voltage mode if V_C exceeds V_{OV}, which disables the boost converter.

Summary. We create models of the chips according to the converter's modes and Eq. 1 and 2. Note that the converter voltages V_H and V_L are fixed values or can be directly computed, while we characterize the converter efficiencies η_H and η_L experimentally and embed them as look-up tables in our models.

B. Modelling DC/DC converters

The modelling of the step-down converter and LDO converter is straight-forward, as they both have only a single operation mode and we thus model them using

$$V_L = min(V_{OUT}, V_C),\ \eta_L = f_{L,DCDC}(V_C, V_L, I_L), \quad (3)$$

where V_{OUT} is a fixed value. Again, we derive look-up tables to model the conversion efficiency η_L.

C. Experimental characterization

We retrieve the converter efficiencies and quiescent current for each IC experimentally according to the BQ25570's guidelines for low-power efficiency measurements [23] and the recommendations in [15]. We use a Keysight B2902B source measurement unit (SMU) for all measurements, as it offers two channels that can source and measure both voltage and current simultaneously with high accuracy. Since each converter characterization requires a sweep across three parameters (i.e., $\{V_C, V_H, I_H\}$ for the boost converter and $\{V_C, V_L, I_L\}$ for the buck converter) with a large numerical range, we control the SMU remotely via Python to perform automated and repeatable measurements[1].

[1]The collected data and scripts for modelling and evaluation as well as additional figures are available at https://doi.org/10.5281/zenodo.10909064.

Boost-conversion efficiency. To retrieve the boost converter efficiency, we configure one SMU channel as a current source to emulate the harvesting source with a given I_H and V_H. The second channel operates as a voltage-controlled current load that resembles the storage capacitor at a given state-of-charge (V_C) and measures the charging current I_C. For each operating point, the boost converter efficiency can then be derived using

$$\eta_H = \frac{V_C \cdot I_C}{V_H \cdot I_H}. \tag{4}$$

We retrieve η_H for each energy harvesting IC for input currents between $50\,\mu A - 10\,mA$, and for voltages across the operating ranges of each IC in steps of $100\,mV$. For the exact configurations, we refer the reader to our artifacts[1].

Buck-conversion efficiency. To obtain the buck converter efficiency, we use one SMU channel to emulate the storage capacitor by configuring it as a voltage source that applies a fixed V_C and measures I_C. The second channel is used as a current sink with a certain I_L, acting as the device's load. The buck converter efficiency can be retrieved using

$$\eta_L = \frac{V_C \cdot I_C}{V_L \cdot I_L}. \tag{5}$$

The boost converter's output voltage V_L is typically configurable, and thus the measurement has to be repeated for each required setting of V_L. We retrieve η_L for the BQ25570 and AEM10941 ICs and both DC/DC converters. Similar to the boost converter measurements, we sweep the voltages and output currents across the entire operating range and use averaging to remove noise from our measurements.

D. Model evaluation

In this section, we evaluate the models of the three energy-harvesting chips and the two buck converters experimentally.

Energy harvesting ICs. To assess the models' accuracy in different operating modes and a realistic scenario, we evaluate the chip's behavior when used with *intermittently operating* IoT nodes. More specifically, we use the two-channel SMU to emulate an energy harvester and a load, and connect a $580\,\mu F$ tantalum capacitor to the IC. We configure all ICs with same MPP factor ($k = 0.8$) and use the internal (BQ25570) or an external (MAX20361, AEM10941) comparator with load switch to enable/disable the buck converter output.

Charging mode. In order to determine the accuracy of the boost- and buck-converter efficiency in charging mode, we pre-charge the capacitor to V_{UV} and use different harvesting and load currents with $I_H < I_L$, such that the capacitor is periodically charged and discharged between V_{High} and V_{Low} (see Fig. 1a), with V_{High} and V_{Low} set according to the ICs' charging mode thresholds. We then measure the charging and discharging time (three times each) to evaluate the model accuracy w.r.t. harvesting and load efficiency, respectively.

We first evaluate the harvesting efficiency by obtaining the charging times for different harvesting currents I_H while the buck-converter is disabled. Fig. 4a shows the measured and simulated charging time at $V_{OC} = 2V$, confirming that our models can accurately describe the harvesting behavior with

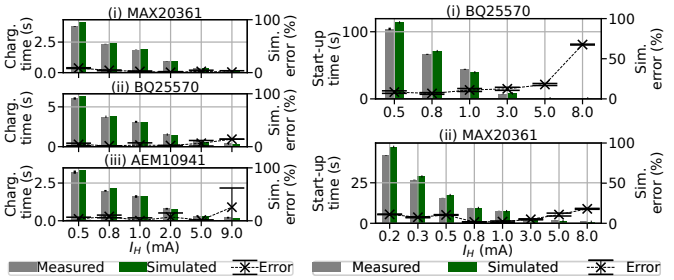

(a) Charging time (b) Start-up time

Fig. 4. Simulated and measured charging (a) and start-up (b) times along with the simulation error for the three energy harvesting ICs.

an average absolute error of 2.9%, 6.5%, and 7.5% for the MAX20361, the BQ25570, and the AEM10941, respectively. In comparison to the MAX20361, the simulation error of the BQ25570 and AEM10941 is higher, which is mainly due to non-deterministic behavior at larger harvesting currents (as visible in the high standard deviation in Fig. 4a-ii and 4a-iii). On the AEM10941, this behavior is caused by its MPP mechanism that only approximates the input voltage V_H within a $50\ mV$ hysteresis. On the BQ25570, the behavior is due to its imprecise internal comparator that causes the output to turn on/off at voltage levels which are not exactly at V_{High}/V_{Low}.

Next, we evaluate the load efficiency by comparing the measured and simulated discharging times at different harvesting and load currents. Note that, in this evaluation, we only use the BQ25570 and AEM10941, as the MAX20361 does not embed a buck converter. We observe average absolute errors as low as 3.5% and 2.7% for the BQ25570 and AEM10941, respectively, across seven different operating points each[1].

Cold-start mode. Finally, we evaluate the accuracy of the models in cold-start mode, i.e., when the chip operates below $V_{IC,min}$. To this end, we obtain the start-up times at different harvesting currents I_H and $V_{OC} = 2V$.We refer to the start-up time as the initial charging time from an empty capacitor to $V_{IC,min}$. In Fig. 4b, the start-up times and the corresponding simulation errors of the BQ25570 and MAX20361 are shown. The average absolute error for the MAX20361 is low (8.3%), while it is rather high for the BQ25570 (20.7%). However, the latter is mainly due to the large errors at high harvesting currents. For $I_H < 5\,mA$, the average error stays below 10%. Unfortunately, we are not able to create a feasible model of AEM10941's cold-start without knowledge of the chip's internal implementation, as its observed behavior is highly dependent on the employed capacitance and non-deterministic. We will further discuss the AEM10941's cold start in Sec. V.

Step-down converter and LDO. To evaluate the buck converter models, we repeat the load efficiency experiments (i.e., measuring the discharge time) for the TPS7A07 and the XC9265. Again, we evaluate different combinations of I_H and I_L and obtain an average error of 3.8% to 5.4% for the TPS7A07 and XC9265, respectively[1]. However, it is worth noting that we observe unstable behavior for the XC9265 step-down converter for large load currents $I_L > 10\,mA$: this IC should thus not be used in this configuration.

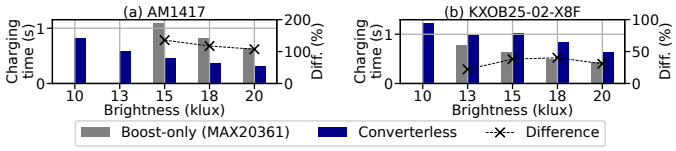

Fig. 5. Comparison of charging times for a boost-only and converter-less architecture for the AM1417 (a) and KXOB25-02-X8F (b) solar panel.

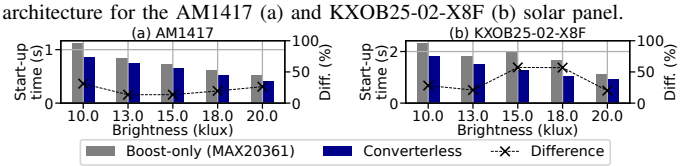

Fig. 6. Comparison of start-up times for a boost-only and converter-less architecture for the AM1417 (a) and KXOB25-02-X8F (b) solar panel.

Summary. Given the evaluation results, we can leverage the proposed models to explore with sufficiently high accuracy the performance of different converter architectures (Sec. IV) and energy-harvesting ICs (Sec. V) in simulation, i.e., without labor-intensive hardware modifications and measurements.

IV. Comparing Converter Architectures

In this section, we explore how the converter architecture affects the device performance in different energy-harvesting scenarios and discuss the corresponding design trade-offs.

A. Converter-less vs. boost-only architecture

We first investigate the effects of a boost converter by comparing a battery-free IoT node connected to its capacitor ($C = 220\mu F$) either without converter or using the MAX20361 (i.e., a boost-only energy harvesting IC).

Impact on energy harvesting efficiency. As the boost converter's purpose is to improve the energy harvesting efficiency by regulating the harvester's voltage to its MPP, we explore the impact on the capacitor's charging time for two solar panels at different (constant) illumination levels. Fig. 5 shows the charging times from $2V$ to $2.8V$. For the Panasonic AM1417 solar panel (see Fig. 5a), the benefits of the boost converter's MPPT mechanism are evident. The capacitor charges more than twice as fast compared to the converterless configuration. Furthermore, charging is possible even for lower illuminance levels, where V_{OC} does not exceed V_{High}. However, for the KXOB25-02-8F solar panel (see Fig. 5b), the converter-less architecture can outperform the boost-only architecture, as the charging time without a converter is 22-40% lower. This behavior is due to the solar panel's P-V characteristic, as shown in Fig. 1b, which aligns well with the voltage threshold configurations. The KXOB25-02-8F's MPP lies between V_{Low} and V_{High} (covered in gray) and it can thus operate close to its optimal operating point even without a boost converter.

Impact on start-up time. As discussed in Sec. II, boost converters suffer from a limited efficiency in cold-start mode, which can lead to long start-up times. For battery-free devices, these start-up times need to be considered, as their small storage capacitors are likely to discharge below the cold-start voltage in periods where no ambient energy is available. We compare the start-up time of a converter-less and boost-only architecture at different illuminance levels in Fig. 6, which shows the time a device with an empty capacitor requires to be operational (i.e., until $V_C = 2\,V$). For both solar panels, the boost-only architecture exhibits increased start-up times by up to 34% and 94%, respectively.

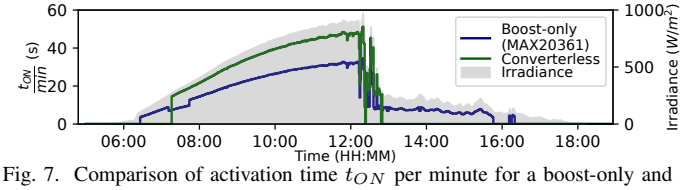

Fig. 7. Comparison of activation time t_{ON} per minute for a boost-only and converter-less architecture using an outdoor energy-harvesting trace.

Comparison using energy-harvesting traces. So far, the comparisons are based on 'static' energy harvesting scenarios, i.e., with a single environmental condition per simulation. To investigate the impact on device performance in a realistic scenario, we now use the simulator's ability to replay energy-harvesting conditions based on recorded irradiance traces and a solar panel model. More specifically, we explore the load performance based on real-world data from the NREL dataset [24] and a Powerfilm LL200-2.4-75 solar panel. Fig. 7 shows the activation time t_{ON} per minute (i.e., the total time the load is enabled and can operate) over an entire day, highlighting an interesting design trade-off. It can be seen that a boost-only architecture allows the node to operate earlier in the morning and also at low-light conditions in the afternoon. On the other hand, the boost-only architecture cannot reach the peak performance at noon and thus, the overall activation time is 20% lower compared to the converter-less architecture.

B. Converter-less vs. buck-only architecture

We explore next the effects of a buck converter and compare the IoT node's performance when the load is connected directly to the capacitor (i.e., converter-less) or using either an LDO (TPS7A02) or a step-down converter (XC9265).

Impact on load efficiency. To this end, we assess the load efficiency by obtaining the time the IoT node can operate without any energy income, given a full capacitor. In other words, we obtain the capacitor's discharge time for $V_C = 3.6$ to $2\,V$ at different (constant) load currents I_L. As shown in Fig. 8 (a), a buck-only architecture using a step-down converter is less efficient at small load currents, but prolongs the discharge time (i.e., operating time) by up to 16% at $I_L > 0.5\,mA$ compared to a converter-less or LDO-based architecture. Additionally, a buck converter allows charging the capacitor to voltages higher than the load's voltage limit. In this case, shown in Fig. 8 (b), the benefits of a step-down converter are even higher, as its efficiency rises with higher input voltages and leads to up to 34% longer operation.

Fig. 8 further shows that the discharge times of the converter-less and LDO-based architecture are almost identical. This is expected, as an LDO simply dissipates power to retain a constant output voltage. Nevertheless, the LDO allows the load to operate at the same voltage regardless of the capacitor's state-of-charge, which is a significant advan-

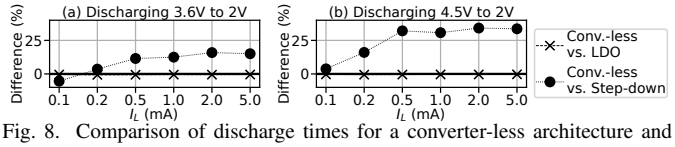

Fig. 8. Comparison of discharge times for a converter-less architecture and two buck-only architectures (i.e., LDO or step-down converter).

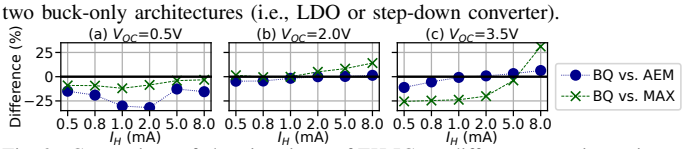

Fig. 9. Comparison of charging times of EH-ICs at different operating points.

tage, as the power consumption of modern CPUs is voltage-dependent [25].

C. Summary and recommendations

In summary, a boost converter should be employed *according to the system's energy harvester, harvesting potential, and application scenario*. More specifically, boost converters are a necessity in challenging energy harvesting environments and if the harvester's voltage does not match the load. However, if the energy harvesting conditions are well known and favorable, a boost-less architecture can be more efficient and, in particular, can decrease start-up times significantly. Furthermore, if cost and size constraints allow, we *always recommend the use of a buck converter*, as it commonly improves the load efficiency and facilitates the overall system modelling.

V. Comparing Energy Harvesting ICs

Sec. IV has shown that voltage converters (i.e., embedded in an EH-IC) are often beneficial or indispensable to power a battery-free device. To support designers in selecting an appropriate IC for their applications, we now simulate and compare three state-of-the-art EH-ICs and discuss their benefits.

Energy-harvesting efficiency. We first explore the efficiency of the ICs' boost conversion by obtaining the charging time in normal operation (i.e., in charging mode). For a fair comparison, we configure each IC with the same MPP factor ($k = 0.6$) and retrieve the charging time from $V_C = 2.5$ to $4V$ (as this lies within the operating range of all three chips). To explore in which ranges the ICs operate best, we simulate a total of 96 operating points for each IC, using different I_H and V_{OC} across the entire operating range. For brevity, Fig. 9 only shows a subset of the results, highlighting the most important trends. At low harvesting voltages (Fig. 9a), the BQ25570 performs best and charges up to 32% and 12% faster than the AEM10941 and MAX20361, respectively. At higher voltages (Fig. 9b and 9c), the BQ25570 and AEM10941 operate very similarly, while the MAX20361 shows the best performance (i.e., decreasing the charging time between 11-14% at large input currents) at $V_{OC} = 2V$. However, the MAX20361 has a very poor efficiency once V_H exceeds 2.6V, as its MPP mechanism does not support higher voltages.

Start-up times. We next compare the start-up times of the ICs from cold-start. As there is no accurate model for the AEM10941's cold-start mode, we rely on experimental data for this comparison. Fig. 10 shows the start-up times of the

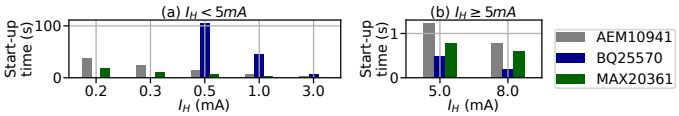

Fig. 10. Large differences in the measured start-up times of three energy harvesting ICs for different input currents and at $V_{OC} = 2V$.

three ICs, when charging from an empty capacitor to $V_C = 2V$ using an SMU with different input currents I_H and an open-circuit voltage of $V_{OC} = 2V$. It can be seen that the BQ25570 has by far the longest start-up times at low currents (i.e., up to $15x$ and $6.2x$ longer compared to the MAX20361 and AEM10941, respectively), and cannot even start operating if $I_H < 0.5\,mA$. This is due to its cold-start mechanism, which offers poor efficiency and regulates V_H to a fixed value of 330 mV, hence limiting the incoming power. Interestingly, for large currents (i.e., $I_H \geq 5mA$), the BQ25570 performs best. Nevertheless, in general, the MAX20361 features the fastest start-up times, as its MPPT mechanism is already fully available once V_C exceeds 350 mV.

Load efficiency. Finally, we compare the efficiency of the ICs' buck conversion when discharging the capacitor from $V_C = 4.5$ to 2.5V at different load currents. The simulation results are not plotted due to space constraints, but they are available in our artifacts[1] and in line with our observations from Sec. IV-B: the BQ25570, embedding a step-down converter, outperforms the AEM10941, as the latter employs an LDO. While the discharge times are very similar for $I_L < 0.5\,mA$, they are 19-25% longer for the BQ25570 at larger currents. The MAX20361 does not employ a buck converter and thus requires additional circuitry to provide a constant output voltage.

A. Summary and recommendations

While the BQ25570 features the highest boost-conversion efficiency at low harvesting voltages and currents, its start-up times are significantly longer. Consequently, we recommend its use mainly in environments where a full discharge of the capacitor is unlikely and cold-start is avoided. In contrast, the MAX20361 offers the lowest start-up times as well as a very reliable and feature-rich MPPT mechanism and is the preferred option for challenging environments where $V_{OC} < 2.6\,V$. As the MAX20361 does not embed a buck-converter, the AEM10941 can be a compromise, due to its acceptable start-up times and the convenience of an integrated LDO.

VI. Related Work

The increasing popularity of battery-free devices has led to the development of many different platforms [19], [26]–[29], dedicated simulators [11]–[14], and models of various device components (e.g., including harvester [30]–[32], capacitor [33]–[35], converter [15] and load [36], [37]).

Existing platforms commonly employ at least one DC/DC converter (i.e., using a boost-only [26], [27], buck-only [19], or boost-buck architecture [28], [29], [38]). Converter-less

platforms are rare and mainly used to demonstrate novel concepts specific to battery-free operation, such as checkpointing strategies [39], [40] or energy storage configurations [41], [42]. Although there exist highly-optimized and complex converter circuits for specific harvesters [43], [44], the majority of battery-free platforms rely on off-the-shelf ICs, such as the MAX20361 [45], the LTC3109 [46], or the popular BQ255xx family [20], [26], [28], [38].

The latter is, to the best of our knowledge, the only energy harvesting IC for which a model is available [15]. While this is pioneering work upon which we build, the model only covers the BQ25570's boost converter efficiency in charging mode, and does neither consider its buck converter nor other operating modes. Besides this work, only limited efforts have been made to compare the different converter architectures, i.e., they are only discussed theoretically [4], [10], or a single architecture is tuned according to the application needs [4].

VII. Conclusions and future work

In this paper, we develop models of three state-of-the-art EH-ICs and two DC/DC converters, evaluate them experimentally, and make them publicly available in an open-source simulation framework for battery-free devices [16]. Furthermore, we use these models to explore the impact of the employed converter architecture and EH-IC on the overall system performance of battery-free devices. We show that the selection is non-trivial, but depends on the given energy harvesting scenario, the used harvester, and the application requirements.

In future work, we plan to extend the investigation using different energy-harvesting scenarios and additional load models. Furthermore, we aim to add new converter models and to include parameter uncertainties within the simulation.

References

[1] J. Hester and J. Sorber, "The Future of Sensing is Batteryless, Intermittent, and Awesome," in *Proc. of the SenSys Conference*, 2017.

[2] Z. Cai *et al.*, "Battery-Free Wireless Sensor Networks: A Comprehensive Survey," *IEEE Internet of Things Journal*, 2023.

[3] J. Hester *et al.*, "Ekho: Realistic and repeatable experimentation for tiny energy-harvesting sensors," in *Proc. of the SenSys Conference*, 2014.

[4] A. Gomez *et al.*, "Dynamic energy burst scaling for transiently powered systems," in *Proc. of the DATE Conference*, 2016.

[5] D. Brunelli *et al.*, "An Efficient Solar Energy Harvester for Wireless Sensor Nodes," in *Proc. of the DATE Conference*, 2008.

[6] Texas Instruments, "BQ25570: Ultra Low power Harvester power Management IC with boost charger, and Nanopower Buck Converter," 2019.

[7] ePeas, "AEM10941: E-peas' solar energy harvesting IC solution," 2023.

[8] Analog Devices, "MAX20361: Small, Single-/Multi-Cell Solar Harvester with MPPT and Harvest Counter," 2023.

[9] STMicroelectronics, "SP1050: Ultra low power energy harvester and battery charger with embedded MPPT and LDOs," 2019.

[10] K. Geissdoerfer *et al.*, "Shepherd: A portable testbed for the batteryless IoT," in *Proc. of the SenSys Conference*, 2019.

[11] S. Sliper *et al.*, "Fused: Closed-Loop Performance and Energy Simulation of Embedded Systems," in *Proc. of the ISPASS Symposium*, 2020.

[12] S. C. Wong *et al.*, "Energy-Aware HW/SW Co-Modeling of Batteryless Wireless Sensor Nodes," in *Proc. of the ENSsys Workshop*, 2020.

[13] H. Brunner *et al.*, "Simba: A Unified Framework to Explore and Facilitate the Design of Battery-Free Systems," in *Proc. of the IPSN Conference*, 2024.

[14] M. Furlong *et al.*, "Realistic Simulation for Tiny Batteryless Sensors," in *Proc. of the ENSsys Workshop*, 2016.

[15] M. Masoudinejad *et al.*, "Average Modelling of State-of-the-Art Ultra-low Power Energy Harvesting Converter IC," in *SPEEDAM Symp.*, 2018.

[16] H. Brunner *et al.*, "Simba simulation framework: Source code." 2024, https://github.com/LENS-TUGraz/simba.

[17] S. T. Sliper *et al.*, "Energy-driven computing," *Philosophical Transactions of the Royal Society*, 2019.

[18] C. Wang *et al.*, "Enhanced charge circuitry for PV energy harvesting with fast activation and high efficiency," *IET Power Elec.*, 2023.

[19] J. de Winkel *et al.*, "Reliable timekeeping for intermittent computing," in *Proc. of the ASPLOS Conference*, 2020.

[20] M. Afanasov *et al.*, "Battery-less Zero-maintenance Embedded Sensing at the Mithræum of Circus Maximus," in *Proc. of SenSys Conf.*, 2020.

[21] Texas Instruments, "TPS7A02: 200mA, nanopower-IQ (25 nA), low-dropout (LDO) voltage regulator with enable," 2019.

[22] Torex, "XC9265: Ultra Low Power Synchronous Step-Down PFM DC/DC Converter," 2019.

[23] Texas Instruments, *User's Guide for bq25570 Battery Charger Evaluation Module for Energy Harvesting*, 2013.

[24] M. Sengupta *et al.*, "The National Solar Radiation Data Base (NSRDB)," *Renewable and Sustainable Energy Reviews*, 2018.

[25] S. Ahmed *et al.*, "Demystifying Energy Consumption Dynamics in Transiently Powered Computers," *Trans. on Emb. Comp. Sys.*, 2020.

[26] K. Geissdoerfer and M. Zimmerling, "Bootstrapping Battery-free Wireless Networks: Efficient Neighbor Discovery and Synchronization in the Face of Intermittency," in *Proc. of the NSDI Symposium*, 2021.

[27] U. Senkans *et al.*, "Applications of Energy-Driven Computing: A Transiently-Powered Wireless Cycle Computer," in *Proc. of the ENSsys Workshop*, 2017.

[28] J. de Winkel *et al.*, "Battery-Free Game Boy," in *Proc. of the IMWUT Conference*, 2020.

[29] F. Fraternali *et al.*, "Pible: Battery-Free Mote for Perpetual Indoor BLE Applications," in *Proc. of BuildSys Conference*, 2018.

[30] S. Vergura, "A Complete and Simplified Datasheet-Based Model of PV Cells in Variable Env. Conditions for Circuit Sim." *Energies*, 2016.

[31] S. Kiran *et al.*, "Modeling, simulation and analysis of piezoelectric energy harvester for wireless sensors," in *Proc. of the ICCEREC Conference*, 2015.

[32] T. Thakuria *et al.*, "Modelling and simulation of low cost RF energy harvesting system," in *Proc. of the IESC Conference*, 2017.

[33] H. Brunner *et al.*, "Leakage-Aware Lifetime Estimation of Battery-Free Sensor Nodes Powered by Supercapacitors," in *ENSsys Workshop*, 2022.

[34] J. Ahn *et al.*, "State-of-Charge Estimation of Supercapacitors in Transiently-Powered Sensor Nodes," *IEEE Transactions on Computer-Aided Design of Integrated Circuits and Systems*, 2022.

[35] G. V. Merrett *et al.*, "Supercapacitor leakage in energy-harvesting sensor nodes: Fact or fiction?" in *Proceedings of the 9th International Conference on Networked Sensing Systems (INSS '12)*, 2012.

[36] A. Arreola *et al.*, "Approaches to Transient Computing for Energy Harvesting Systems: A Quantitative Eval." in *ENSsys Workshop*, 2015.

[37] J. S. Miguel *et al.*, "The EH Model: Early design space exploration of intermittent processor architectures," in *Proc. MICRO Symposium*, 2018.

[38] J. de Winkel *et al.*, "Intermittently-Powered that Works," in *Proc. of the MobiSys Conference*, 2022.

[39] D. Balsamo *et al.*, "Hibernus: Sustaining computation during intermittent supply for energy-harvesting systems," *Emb. Systems Letters*, 2015.

[40] K. Maeng and B. Lucia, "Adaptive low-overhead scheduling for periodic and reactive intermittent execution," in *Proc. SIGPLAN Conf.*, 2020.

[41] J. Zhan *et al.*, "Exploring the Effect of Energy Storage Sizing on Intermittent Computing System Performance," *IEEE Trans. on Computer-Aided Design of Integrated Circuits and Systems*, 2022.

[42] J. Hester *et al.*, "Tragedy of the Coulombs: Federating Energy Storage for Tiny, Intermittently-Powered Sensors," in *Proc. of the SenSys Conference*, 2015.

[43] S. Bose *et al.*, "Integrated Cold Start of a Boost Converter at 57 mV Using Cross-Coupled Complementary Charge Pumps and Ultra-Low-Voltage Ring Oscillator," *IEEE Journal of Solid-State Circuits*, 2019.

[44] S. Bandyopadhyay *et al.*, "A 1.1 nW Energy-Harvesting System with 544 pW Quiescent Power for Next-Generation Implants," *IEEE Journal of Solid-State Circuits*, 2014.

[45] Nessie Circuits, "Riotee: An open-source platform for the battery-free IoT," [Online] https://tinyurl.com/38m5nhw6 – Last access: 2023-10-02.

[46] B. Campbell *et al.*, "Energy-harvesting thermoelectric sensing for unobtrusive water and appliance metering," in *Proc. of the ENSsys Workshop*, 2014.